International Institute for
Applied Systems Analysis
Schlossplatz 1
A-2361 Laxenburg, Austria

Tel: +43 2236 807 342
Fax: +43 2236 71313
E-mail: publications@iiasa.ac.at
Web: www.iiasa.ac.at

Interim Report **IR-09-056**

Impacts of agricultural expansion on irrigation water requirements in Taita hills, Kenya

Eduardo Eiji Maeda (eduardo.maeda@helsinki.fi)

Approved by

Marek Makowski (marek@iiasa.ac.at)
Leader, Integrated Modeling Environment Project

October, 2009

Foreword

This report describes the research carried out by the author during participation in the Young Scientists Summer Program 2009 (YSSP) with the Integrated Modeling Environment Project. The research documented in this report is part of a long-term study that the author has been carrying out at the University of Helsinki as part of his Ph.D. research. The objective of the author's Ph.D. research is to evaluate the interactions between agricultural expansion and climate change in East Africa in order to outline adaptation strategies towards food security and water resources management. Such research is being supervised by Prof. Petri Pellikka, leader of the Geoinformatics research group located in the Department of Geography at the University of Helsinki.

The goal for this three months summer program was to assemble an integrated modeling framework comprising a Land Use and Land Cover Change (LUCC) model and an Evapotranspiration (ET) model in order to evaluate the impacts of agricultural expansion on irrigation water requirements in Taita Hills, SE-Kenya. Such research contributed for the author's long-term goals by improving the understanding on the water resources requirements in this particular region and by assembling a methodology that will be extended to other regions in East Africa. The results achieved within these three months will also be directly used as inputs for the subsequent parts of the author's research, which will aim to evaluate how changes in irrigation water requirement may affect agricultural productivity in the region.

Abstract

The presented work aims to evaluate the impacts of agricultural expansion on irrigation water requirements in Taita Hills, SE-Kenya. The first procedure of this research consists in implementing and calibrating an Evapotraspiration (ET) model for the study area. The ET is an important component of the hydrological cycle and an accurate quantification of such component is crucial for the design, operation and management of irrigation systems. Three temperature based ET models are evaluated, namely the Hargreaves, the Thornthwaite and the Blaney-Criddle, given that these are the most recommended approaches when only air temperature data are available at weather stations. To overcome the insufficient data retrieved from ground stations, remote sensing land surface temperature data are used as input for the models. One weather station with complete climate datasets is used to calibrate the selected model using as reference the FAO-56 Penman–Monteith method. Simultaneously, future land use scenarios are simulated using a Land Use and Land Cover Change (LUCC) model. Synthetic weather datasets (temperature and precipitation) are generated using a Monte Carlo simulation. Finally, the ET model and the LUCC model are integrated into a modeling framework in order to delineate Irrigation Water Requirement (IWR) scenarios. The simulations indicate that throughout the next 20 years the low availability of space in highlands will drive agricultural expansion to areas with higher IWR in the foothills. However, climate changes predicted by GCMs will likely decrease IWR when compared with scenarios using the same temperature and precipitation averages as in the historical dataset.

Acknowledgments

I would like to express my gratitude to the entire Integrated Modeling Environment Project team, especially to Dr. Marek Makowski, for his constant support and attention given to the IME YSSPeers. Another special thank you goes to my YSSP colleague Luciana Kindl da Cunha, for the interesting and fruitful discussions on technical and not- so- technical issues. I also would like to thank Dr. David Wiberg and Dr. Tatiana Ermolieva for their comments and suggestions on my research.

Thanks for Prof. Petri Pellikka, Mika Siljander and Barnaby Clark from the University of Helsinki for providing part of the data used in this research.

My participation on the YSSP was funded by the Academy of Finland, for which I am greatly thankful.

About the Author

Eduardo Maeda is a Ph.D. student in Physical Geography at the University of Helsinki, Finland. He holds a BSc in Agricultural and Environmental Engineering from the Federal University of Viçosa, Brazil, with a training period at the Iowa State University, USA. He completed his MSc in Remote Sensing at the National Institute for Space Research, Brazil in 2008.

Contents

Table of Figures

Impacts of agricultural expansion on irrigation water requirements in Taita hills, Kenya

Eduardo Eiji Maeda* ** (eduardo.maeda@helsinki.fi)

1. Background and motivation

Currently roughly 70% of freshwater withdraws are used for agriculture (FAO, 2005). Although global withdrawals of water resources are still below the critical limit, more than two billion people live in highly water-stressed areas due to the uneven distribution of this resource in time and space (Oki and Kanae, 2006). In Kenya, over 55% of the rural population does not have access to quality drinkable water (FAO, 2005). Simulated scenarios indicate that up to 59% of the world population will face some sort of water shortage by 2050 (Rockstrom et al., 2009).

In this context, the accurate assessment of water demand and distribution is crucial to improve water management. In most Sub-Saharan African countries agriculture is the main economic activity, representing around 40% to their gross domestic product (Barrios et al. 2008). Consequently, the water use for irrigation in such regions must be carefully controlled and future trends in the expansion of agricultural areas should be considered during policy decisions.

The improvement of models and computer capacity in the past decades facilitated an increasing number of studies aiming the sustainable use of water resources and land use planning. For instance, Land Use and Land Cover Change (LUCC) models are extensively used to represent the complexity of land use systems in agricultural and urban areas. Such models are considered to be important tools to project alternative scenarios into the future and to test our understanding of the LUCC process (Veldkamp and Lambin, 2001). A good knowledge of the circumstances and driving forces of agricultural expansion is an essential step for elaborating public policies that can effectively lead to the conservation of natural resources.

In irrigation water management, the use of Hydrometeorological models to estimate crop Evapotranspiration (ET) results in important contributions at global, regional and local scales. ET is defined as the combination of two separate processes, in which water is lost on the one hand from the soil surface by evaporation and on the other hand from the crop by transpiration (Allen et al., 1998). Quantification of ET is needed by water managers for the design, operation and management of irrigation systems (Mohan and Arumugam, 1995).

Although many studies have been undertaken to understand each of these processes, scientists are facing today the challenge to integrate or couple these models into more complex frameworks in order to better understand the interconnected relations between socioeconomic factors and the environment. Water resources, agricultural production and land use are closely linked with each other, with local climate and with society, assembling a very complex system. The design of a modelling framework able to perform an integrated analysis and assessment of this system, therefore, is a complex process.

---

*Integrated Modeling Project, IIASA
**University of Helsinki

One of the problems commonly faced in the integration of ET models into spatially explicit modelling frameworks is the lack of high spatial resolution weather data retrieved from ground stations. Therefore, the combination of ET models with remote sensing data provides a feasible alternative to obtain temporally and spatially continuous information about biophysical variables. According to Wagner et al. (2008), in poorly gauged catchments, remote sensing data can significantly improve the availability of necessary information, for instance albedo, leaf area index and Land Surface Temperature (LST) (Wan, 2008).

My study addresses the insufficient weather data from ground stations by incorporating remote sensing data into an empirical ET model for the region of Taita Hills, SE-Kenya. The ET model is calibrated and then integrated with a spatially explicit LUCC model in order to delineate irrigation water requirements scenarios for the study area.

1.1 Goal

Evaluate the impacts of agricultural expansion on irrigation water requirements in Taita Hills, SE-Kenya.

1.2 Research questions

- Will future climate patterns (e.g. rainfall, temperature) potentially increase irrigation water requirements?
- Which regions inside the study area will experience higher water resources demand for agricultural production by 2030?
- Can Remote sensing data (LST) be used to estimate evapotranspiration in this study area?
- Which is the most appropriate model to estimate ETo in this study area?

2. Study area

Taita Hills is the northernmost part of the Eastern Arc Mountains, situated in the middle of the Tsavo plains of the Taita-Taveta District in the Coast Province, Kenya (Figure 1). Taita Hills cover an area of 1000 km2. The land use in the region is dominated by intensive agriculture, while extensive agriculture and grazing are dominant land use types on the foothills and plains.

The population of the whole Taita-Taveta district has grown from 90,146 (1962) persons to over 300,000 (Republic of Kenya, 2001). The indigenous cloud forests of the Taita Hills, which are of great importance for conservation, have suffered substantial loss and degradation since the early 1960s. The hills were forested only a few hundred years ago above the elevation of 1400 meters on the southern and eastern slopes. Today, only 1% of the forested area remains.

The area is considered to have high scientific interest, and there is a high potential for succeeding in the connectivity development and community-based natural resource management.

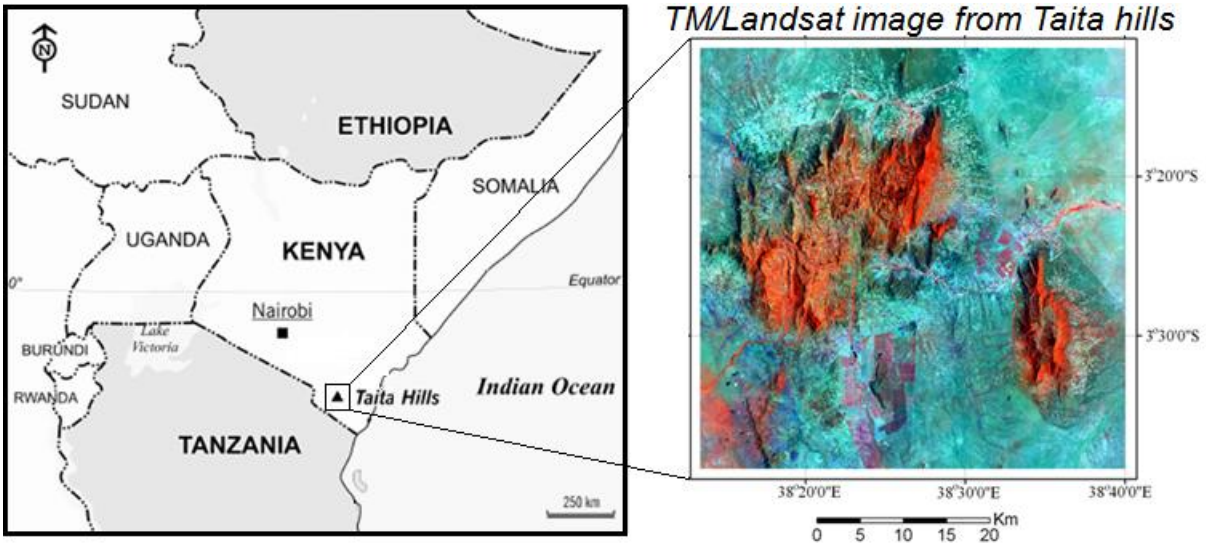

Figure 1. Geographic location of the study area.

3. Methods

A Land Use and Land Cover Change (LUCC) model and an Evapotranspiration (ET) model were integrated in order to assemble the modelling framework for this study case. To achieve this final framework, the following specific steps were performed:

- Identification of the most appropriate Reference ET (ETo) model for the study area.
- Assimilation of MODIS sensor LST data as input for the ETo model
- ETo model Calibration
- Identification of the agricultural calendar and temporal distribution of crop phenology using remote sensing data
- Attribution of crop coefficients based on crop phenology
- Delineation of LUCC scenarios
- Integration of the ET model with the LUCC model
- Delineation of irrigation water requirement scenarios

The flowchart presented in Figure 2 illustrates the concept of the modeling framework assembled in the present study.

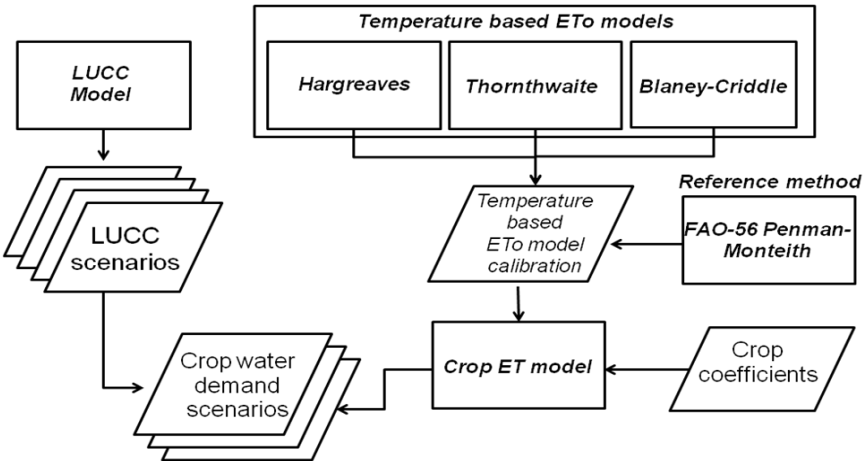

Figure 2. Integrated modeling framework concept

3.1 LUCC model

A spatially explicit simulation model of landscape dynamics, DINAMICA-EGO (Rodrigues et al., 2007; Soares-Filho et al., 2007), was used in order to model the agricultural expansion in the study area and simulate future scenarios of land use. A general description of the LUCC model is presented in Figure 3.

The model receives as inputs land use transition rates, landscape variables and landscape parameters. The landscape parameters are usually intrinsic spatially distributed features, such as soil type and slope, which are kept constant during the simulation process. The landscape variables are spatial-temporal dynamic features that are subjected to changes by decision makers, for instance roads and protected areas. The land use transition rates were also considered to be decision variables, giving that the integrated modelling framework was designed based on the assumption that agricultural expansion rates can be modified by public policies or other external forces.

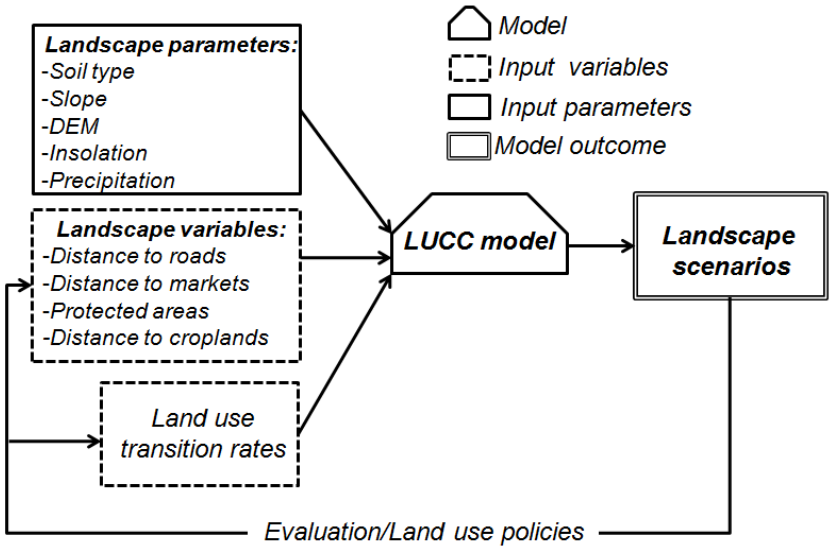

Figure 3. LUCC model description

The DINAMICA-EGO model uses the weights of evidence (WoE) method, which is entirely based on the Bayes' theorem, in which the effect of each landscape variable on a land use transition is calculated independently of a combined solution. The spatial probability of a land use transition is given by the following equation (Bonham-Carter, 1994):

$$\mathrm{P}_{\mathrm{x,y}}\{T/V_1 \cap V_2 \cap ... \cap V_n\} = \frac{O\{T\} \times e^{\sum_{i=1}^{n} W^{+}_{x,y}}}{1 + O\{T\} \times \sum_{j=1}^{t} e^{\sum_{i=1}^{n} W^{+}_{x,y}}} \quad (1)$$

where:

$P_{x,y}$ = probability of transition in a cell with coordinates x,y;

T = land use/land cover transition;

V_i = landscape variables i selected to explain transition T;

$O\{T\}$ = odds of a transition, represented by the ratio between a determined transition probability and the complementary probability of non-occurrence:

$$\mathrm{O\{T\}} = \frac{\mathrm{P\{T\}}}{\mathrm{P\{\overline{T}\}}} \quad (2)$$

where:

$P\{T\}$ = probability of occurring transition T, given by the number of cells where the concerned land use/land cover transition occurred divided by the total number of cells in the study area;

$P\{\overline{T}\}$= probability of not occurring transition T, given by the number of cells where the concerned land use/land cover transition is absent divided by the total number of cells in the study area;

$W^{+}_{x,y}$ = weight of evidence for a determined landscape variable range, defined by the following equation:

$$W^{+} = \log_e \frac{P\{Vi/T\}}{P\{Vi/\overline{T}\}} \quad (3)$$

where:

$P\{V_i/T\}$ = probability of occurring variable V_i in face of the previous presence of transition T, given by the number of cells where both V_i and T are found divided by the total number of cells where T is found;

$P\{V_i/\overline{T}\}$ = probability of occurring variable V_i in face of the previous absence of transition T, given by the number of cells where both V_i and $\overline{T}$ are found divided by the total number of cells where T is not found.

3.1.1 LUCC model internal parameters calibration

DINAMICA-EGO renders two transition algorithms responsible for the allocation of the land use/land cover changes: *expander* and *patcher*. The *expander* function performs

the expansion of previously existing patches of a certain class. The *patcher* function, in its turn, is designed to generate new patches through a seed formation mechanism (Soares-Filho et al., 2002). Therefore, the first parameter to be calibrated in the simulation is the percentage of changes that will be addressed by each of these two algorithms. For instance, in regions where the landscape changes happen exclusively by the expansion of existing patches, the changes should be 100% arranged by the expander function.

The next parameters to be adjusted are the mean and variance of the new patches sizes. These parameters can be independently adjusted for the *expander* and *patcher* functions. The model also includes another heuristic parameter denominated patch isometry index. A high isometry index results in compact patches, while low values are reflected in more fragmented formations.

3.1.2 LUCC model validation

The model performance was evaluated using an adaptation of the method proposed by Hagen (2003), in which multiple resolution windows are used to compare the simulated and the reference maps within a neighbourhood context. The adaptation consists on the fact that each type of change is analysed separately using pairwise comparisons involving maps of differences: (i) between the initial land use/land cover map and a simulated one, and (ii) between the same initial land use/land cover map and the reference one.

Approaches considering neighbourhood contexts are useful in comparing maps that do not exactly match on a cell-by-cell basis, but still present similar spatial patterns within certain cell vicinity (Soares-Filho et al., 2002). The method retrieves a fuzzy similarity index defined inside a window that is gradually expanded, allowing the assessment of the model performance at multiple spatial resolutions.

3.2 Reference Evapotranspiration (ETo) Models

The first step towards the estimation of Crop ET (ETc) is to calculate the Reference ET (ETo). ETo is defined as the ET rate from a reference surface, where the reference surface represents hypothetical grass with specific and well known characteristics (Allen et all, 1998). The concept of ETo was introduced to study the evaporative demand of the atmosphere independently of crop type, crop phenology and management practices.

Several empirical and physical based ETo models have been developed along the last decades, varying in complexity and data requirement. The FAO-56 Penman–Monteith (FAO-PM) equation is considered the standard and most precise method for calculating ETo. Nevertheless, this method demands very detailed meteorological data, which are frequently missing from meteorological stations (Jabloun and Sahli, 2008). In addition, setting up stations capable to record the data required by the FAO-PM method is highly costly. To overcome this problem, three ET models that requires only air temperature data were evaluated, namely, the Hargreaves, the Thornthwaite and the Blaney-Criddle. One synoptic station with complete meteorological data sets was used to calibrate the models using as reference the FAO-PM method.

An overall illustration of the Crop evapotranspiration models is presented in Figure 4. In the particular case of this study, the climatological entities were

considered to be parameters of the model. These parameters were changed during different simulation in order to generate alternative scenarios.

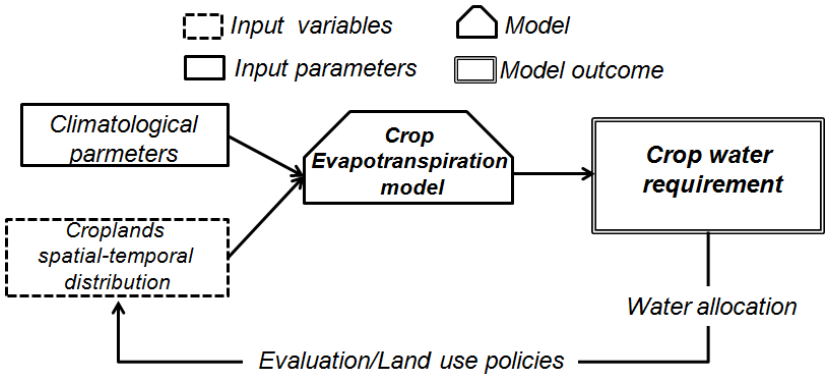

Figure 4. Crop evapotranspiration model description

The ETo models used in this study are described in details below.

A) ***FAO-56 Penman-Monteith method:***

The FAO Penman–Monteith (FAO-PM) method is recommended as the standard ETo method and has been accepted by the scientific community as the most precise one for its good results when compared with other equations in different regions worldwide (Cai et al., 2007; Jabloun and Sahli, 2008). The equation is given by (Allen et al., 1998):

$$ETo = \frac{0.408\Delta(Rn - G) + \gamma \frac{900}{T + 273} u_2 (e_s - e_a)}{\Delta + \gamma(1 + 0.34u_2)} \quad (4)$$

where:

Rn = net radiation at the crop surface [MJ m-2 day^{-1}]; G = soil heat flux density [MJ m-2 day^{-1}]; T = mean daily air temperature at 2 m height [°C]; u_2 = wind speed at 2 m height [m s^{-1}]; e_s = saturation vapour pressure [kPa]; e_a = actual vapour pressure [kPa]; e_s - ea = saturation vapour pressure deficit [kPa]; D = slope vapour pressure curve [kPa °C^{-1}]; γ = psychrometric constant [kPa °C^{-1}].

B) ***Hargreaves:***

The Hargreaves method has been developed by Hargreaves et al. (1985) to overcome the lack of detailed weather data usually required for complex models such as the FAO-PM. The Hargreaves equation requires only daily mean, maximum, minimum air temperature and extraterrestrial radiation. The equation can be written as:

$$ETo = 0.0023 \cdot RA \cdot \left((T\max - T\min)^{0.5} \cdot (Tmean + 17.8)\right) \quad (5)$$

where:
RA = extraterrestrial radiation; Tmean = Mean temperature; Tmin = Minimum temperature; Tmax = Maximum temperature

C) ***Thornthwaite:***

The Thornthwaite method (Thornthwaite, 1948) is based on an empirical relationship between ETo and mean air temperature. The value of ETo for a standard month of 30 days, as a function of the monthly average temperature is given by the following equations:

$$ETo = 16\left(10\frac{Tmean}{I}\right)^{a} \quad (6)$$

$$I = \sum_{i=1}^{12}\left(\frac{t_i}{5}\right)^{1,514} \quad (7)$$

$$a = 67{,}5.10^{-8} I^3 - 7{,}71.10^{-6} I^2 + 0{,}01791 I + 0{,}492 \quad (8)$$

where:

I = thermal index imposed by the local normal climatic temperature regime.

D) ***Blaney-Criddle:***

The Blaney-Criddle equation (Blaney and Criddle, 1962), which was modified by Doorenbos and Pruitt (1977) is one of the first empirical models developed to estimate ETo. Although it was developed some decades ago, this method is still successfully applied in many water management studies (e.g. Loukas et al., 2005; Fooladmand and Ahmadi, 2009). The Blaney-Criddle equation is given by:

$$ETo = p \cdot (0.46 \cdot Tmean + 8.13)) \quad (9)$$

where:

p= Mean daily percentage of annual daytime hours for different latitudes

3.2.1 Input data

The common approach used for modelling ETo is to use weather data retrieve from ground meteorological stations as input for the models. However, even when using simpler models that require only air temperature, the data available from ground stations may not be sufficient to represent the spatial distribution of the ET process in detailed scales. To overcome this problem, Land Surface Temperature (LST) data obtained by the Moderate Resolution Imaging Spectroradiometer (MODIS) were used as input to the ETo models. The MODIS sensor (Justice et al., 2002), launched in 1999 and 2002 on board of the Terra and Aqua satellites, respectively, retrieves almost daily LST data. This study made use of the MOD11A2 product (Wan, 2008), which offers day-time and night-time LST data stored on a 1-km Sinusoidal grid as the average values of clear-sky LSTs during an 8-day period.

In total, 368 LST images, corresponding to the entire MOD11A2 product dataset from the years 2001 to 2008, were downloaded from the Land Processes Distributed Active Archive Center (LP DAAC). The 1-km resolution grids were interpolated by kriging in order to reach the same spatial scale as the land use maps (20m). The parameters necessary to carry out the kriging (i.e. nugget, lag size, major range and partial sill) were defined by geostatistical analyses performed in annual average LST images.

3.2.2 ETo models calibration and error assessment

Many studies have been reported along the last years applying the Hargreaves, the Thornthwaite and the Blaney-Criddle models (Gavilán et al., 2006, Ahmadi and Fooladmand, 2008, Fooladmand and Ahmadi, 2009). The results of such studies clearly mention that although those models were effective in estimating ETo, the empirical nature of these methods makes necessary rigorous local calibration.

Hence, the empirical equations were calibrated using as reference the FAO-PM method. It is important to note that the FAO-PM method does not necessarily retrieve real ETo values, due to the uncertainties and errors associated with this method. However, the FAO-PM has proved to behave well under a variety of climatic conditions, and for this reason the use of such method to calibrate or validate empirical equations has been widely recommended (Allen et al., 1998; Itenfisu et al., 2003; Gavilán et al., 2006).

The meteorological data necessary for the FAO-PM equations were obtained from a synoptic station placed at Voi municipality at an altitude of 597 meters, longitude 38.34o E, and latitude 3.24o S. ETo values were calculated for this exact point using the empirical models and MODIS LST data. The calibration parameters were defined using the following equation (Allen et al., 1998):

$$ETo_R = a + b \cdot ETo_T \tag{10}$$

Where ETo_T represents the ETo values estimated using the temperature based models, ETo_R represents the ETo values calculated using the reference method (FAO-PM), and a and b are the calibration parameters.

The models were compared using standard statistics and linear regression analysis (Douglas et al. 2009). Root Mean Squared Error (RMSE) and Mean Absolute Error (MAE) were computed using the equations described below:

$$RMSE = \left(\frac{1}{n} \sum_{1}^{n} \left(ETo_T - ETo_R \right)^2 \right)^{0.5} \tag{11}$$

$$MAE = \frac{1}{n} \sum_{1}^{n} \left| ETo_T - ETo_R \right| \tag{12}$$

3.3 Crop coefficients (Kc)

In order to calculate the Crop Evapotranspiration (ETc) for a determined ETo condition, the ETo value has to be multiplied by a crop coefficient (Kc). Consequently, the Kc incorporates into the equation the crop type, variety and development stage, enabling the representation of the spatial-temporal distributions of croplands. In general, three Kc values are required to describe the crops temporal distribution during an agricultural season: those during the initial stage (Kci), the mid-season stage (Kcm) and at the end of the late season stage (Kce).

The Kc values used in the present study were obtained from tables recommended by FAO (Allen et al., 1998). Nevertheless, to assign the appropriate Kc values it is essential to identify the agriculture calendar in the study area, that is, the period of the year when crops are planted, grown and harvested. For this, monthly Normalized Difference Vegetation Index (NDVI) obtained from satellite images were used to retrieve the phenological stages of croplands.

The NDVI imagery were obtained from the MOD13Q1 product (Justice et al., 2002), which provides 16-day composite imagery from the MODIS Terra/Aqua sensors. The MODIS sensor, launched in 1999 and 2002 on board of the Terra and Aqua satellites, respectively, offers almost daily imagery with a spatial resolution of 250m in the visible red and near-infrared wavelengths. These bands were specifically designed to detect land cover change dynamics (Townshend and Justice 1988). After the NDVI imagery were acquired, random points were distributed along the agricultural areas. The monthly average NDVI values in each of these points were observed throughout the year, in order to identify the development stage of crops.

A drawback of this approach is the fact that the spatial resolution of the MODIS NDVI imagery may be sometimes too coarse to represent agricultural patches from small farms. To overcome this problem and reduce the effect of pixel mixture, a selection was carried out in the random points in order to choose just the ones located over “pure” pixels in agricultural areas. This task was performed based on the Pixel Purity Index (PPI), which aim is to find the most spectrally pure pixels in multispectral and hyperspectral images. The PPI is computed by repeatedly projecting n-dimensional scatter plots on a random unit vector. The extreme pixels in each projection (those pixels that fall onto the ends of the unit vector) are recorded and the total number of times each pixel is marked as extreme is memorized. A Pixel Purity Image is created where each pixel value corresponds to the number of times that pixel was recorded as extreme (Boardman et al., 1994).

3.4 Irrigation water requirement

Crop water requirement (CWR) is defined as the amount of water required to compensate the evapotranspiration loss from the cropped field (Allen et al., 1998). In cases where all the water needed for optimal growth of the crop is provided by rainfall, irrigation is not required and the Irrigation Water Requirement (IWR) is equals to zero. In cases where all water has to be supplied by irrigation the IWR is equals to the CWR (ETc). However, when part of the CWR is supplied by rainfall and the remaining part by irrigation, the IWR is equal to the difference between the ETc and the Effective Precipitation (Peff). In such cases, the IWR was computed using the following equation (FAO, 1997):

$$IWR_m = \left(Kc_m \times ETo_m \times 30\right) - Peff_m \quad (13)$$

where:

IWR m = Monthly average crop water requirement in month *m,* [mm]

Kc_m = Crop coefficient in month *m,* [ ]

ETo_m = Mean daily reference evapotranspiration in month *m,* [$mm.day^{-1}$]

$Peff_m$ = Average effective precipitation in month *m,* [mm]

The P_{eff} is defined as the fraction of rainfall retained in the root zone, which can be effectively used by the plants. That is, the portion of precipitation that is not lost by runoff, evaporation or deep percolation (Brouwer and Heibloem, 1986). The monthly total rainfall was converted to P_{eff} values using Table 1.

Table 1. Conversion table used to define the monthly effective precipitation

P (mm/month)	Peff (mm/month)	P (mm/month)	Peff (mm/month)
0	0	130	79
10	0	140	87
20	2	150	95
30	8	160	103
40	14	170	111
50	20	180	119
60	26	190	127
70	32	200	135
80	39	210	143
90	47	220	151
100	55	230	159
110	63	240	167
120	71	250	175

Source: Brouwer and Heibloem (1986)

3.5 Scenarios simulation

Two climate scenarios and two LUCC scenarios were combined into the modeling framework in order to simulate four IWR scenarios. Each of these scenarios is described in detail below.

a) Climate Scenarios

Without Climate Change: in this scenario, a Monte Carlo simulation was performed in order to generate synthetic temperature and precipitation monthly datasets using a normal distribution with the same average and standard deviation as observed in the historical datasets.

It is important to emphasize that using a normal distribution to describe the temperature and precipitation patterns is a simplified approach, given that these

natural processes do not necessarily follow this kind of distribution. The estimation of a site specific distribution for temperature and precipitation is itself a complex problem, which was not addressed during this study.

With Climate Change: following the same strategy as in the previous scenario, a Monte Carlo simulation was performed in delineating a climate change scenario. However, in this case, the averages of the normal distributions representing temperature and precipitation were gradually changed along the simulation. These changes in the normal distribution averages were based in projections from a set of 21 General Circulation Models (GCMs) for the A1B scenario, reported in the IPCC 4th assessment report. The mean responses in temperature (^{o}C) and precipitation (%) for the period 2011-2030 obtained by the GCMs were considered. As the spatial resolution of such models are coarser than the resolution in which the present study was carried out, only the grid point closest to the centre of the study area was considered for each GCM.

Hence, it is fundamental to state that the aim of this approach was not to perform a spatial downscale in the GCMs outputs, but rather use its result to ground plausible changes in temperature and precipitation monthly averages taken from historical datasets at a better spatial resolution.

The A1B scenario assumes “A future world of very rapid economic growth, low population growth and rapid introduction of new and more efficient technology. Major underlying themes are economic and cultural convergence and capacity building, with a substantial reduction in regional differences in per capita income. In this world, people pursue personal wealth rather than environmental quality” (IPCC, 2007).

b) LUCC scenarios

Business as Usual: This scenario was simulated using an exploratory approach. An exploratory scenario is a sequence of emerging events (Alcamo, 2001). In the particular case of this work, the average agricultural expansion rates observed from 1987 to 2003 in the study area were used to build an exploratory scenario with stationary behaviour for the year 2030. Hence, in this case agricultural expansion rates are not affected by climate changes and just one LUCC scenario is retrieved from the simulation.

Governance: In this case, a prescriptive scenario was simulated. Prescriptive scenarios are established a priori by the modeler in accordance with a targeted future (Alcamo, 2001). Thus, the agricultural expansion rates were associated to fictitious governance policies, in which the LUCCs were constrained according to the availability of Renewable Freshwater Resources (RWR). RWR is defined as the water that is continuously recharged in the hydrological cycle. In the particular case of this work was represented by the annual average rainfall volume.

The assumption made was that annual IWR could not exceed 70% of the total RWR, leaving the remaining 30% to be used by residential or commercial purposes. Consequently, the agricultural expansion rates were gradually decreased along the simulated years as the IWR would approach the RWR limit. The 70% threshold was based on the global average distribution of water resources withdraws (FAO, 2005) and used as a virtual limit of water consumption. This approach, however, does not represent any real policy or water management strategies. The equation used to calculate the transition rates is written as follows:

$$R_{yab} = \frac{\left(R_{i\,ab} \times IWR_y\right) - \left(0{,}7 \times RWR \times R_{i\,ab}\right)}{\left(IWR_i - 0{,}7 \times RWR\right)} \quad (14)$$

where:

R_{yab} = transition rate from *a* to *b* along the year *y*.

R_{iab} = transition rates for the same land use types in the beginning of the simulation.

IWR_y = annual average irrigation water requirements during year *y*.

IWR_i = annual average irrigation water requirements in the beginning of the simulation.

RWR = annual average renewable freshwater resources.

Because in this case transition rates vary with IWR, different climate conditions result in different LUCC scenarios. Hence, when facing a scenario with climate change, the IWR and RWR are gradually changed. These changes are reflected in the agricultural expansion rates, which consequently result in a different LUCC scenario.

3.5.1 Irrigation water requirement scenarios

The LUCC scenarios and the climate scenarios were integrated in the modeling framework, resulting in four IWR scenarios. This integration is represented in Figure 5, and briefly described below.

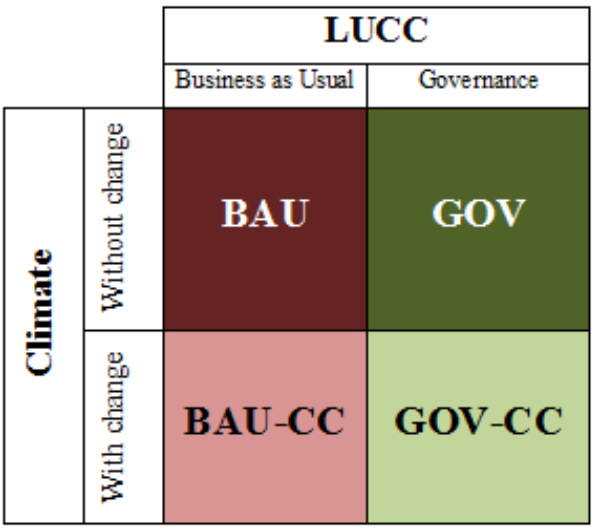

Figure 5. Irrigation water requirement scenarios simulated in the present work.

BAU: IWR for an agricultural area expanding at the same rates observed from 1987 to 2003, and inserted in a climate scenario with the same average and variance as observed in the historical dataset available.

BAU-CC: IWR for an agricultural area expanding at the same rates observed from 1987 to 2003, and inserted in a climate scenario where the temperature and precipitation averages gradually change in a similar level as indicated in the A1B scenario.

GOV: IWR for an agricultural area which expansion rate is controlled based on the availability of renewable freshwater resources. Such agricultural activities are inserted in a climate scenario with the same average and variance as observed in the historical dataset available.

GOV-CC: IWR for an agricultural area wherein expansion rate is controlled based on the availability of renewable freshwater resources. Such agricultural activities are inserted in a climate scenario where the temperature and precipitation averages gradually change in a similar level as indicated in the A1B scenario.

4. Results

4.1 LUCC scenarios

The annual average agricultural expansion rates observed from 1987 to 2003 are shown in Table 2. The highest conversion rates were observed in the transition from woodlands to agriculture. However, shrublands areas are the most affected considering absolute numbers, given that it currently represents the predominant vegetation type in the region. The small regions covered with Broadleaved Forests were nearly untouched, presenting low conversion rates, the total area passed from 7.7 to 6.9 km^2 , along the observed period.

Table 2. Annual average agricultural expansion rates (baseline 1987-2003)

Original vegetation	**Annual conversion rate (%)**
Shrubland	1.305
Woodland	2.013
Plantation Forest	1.161
Broadleaved Forest	0.289
Grassland	0.310

The evaluation of the LUCC model performance is illustrated in Figure 6, which shows the fuzzy similarity indexes achieved using different widow sizes. The maximum fuzzy similarity indices ranged from around 55% at a spatial resolution of 20 m to 90% at a spatial resolution of 380m.

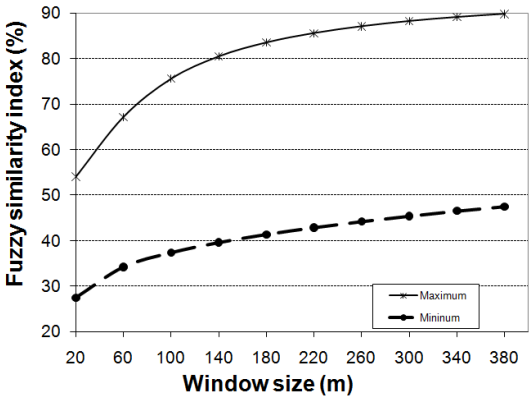

Figure 6. Fuzzy similarity indexes based on multiple size windows.

After the model was calibrated and the role of each landscape variable was defined, transition probability maps were created for each simulated year. In Figure 7, and example of a transition probability map for the year 2003 is illustrated. In the map, the light colors represent areas with higher probability of having the original vegetation converted into croplands. Once spatial probabilities are defined, the new agricultural patches are stochastically allocated by the "*expander*" and "*patcher*" algorithms.

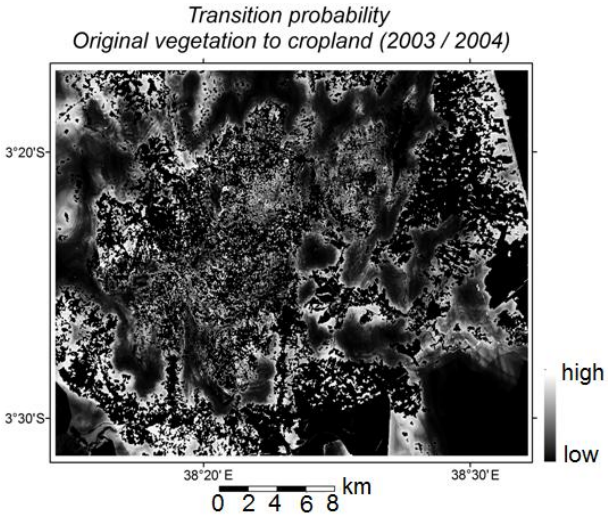

Figure7. Original vegetation to cropland transition probability map for 2003.

The numerical results of the simulations are presented in Figure 8, which displays the total cropland areas in the study site from 2010 to 2030. In the BAU scenario, the cropland areas expanded to around 515 km^2 in 2030, corresponding to about 60% of the study area. This represent an increase of 40% in comparison to the year 2003, when croplands occupied around 365 km^2. The GOV scenario showed the lowest increase in cropland areas, reaching 488 km^2 in 2030.

The GOV-CC scenario, in turn, had agricultural expansion rates slightly higher than the GOV scenario, finishing 2030 with around 495 km^2 in cropland areas. This result is explained by the fact that changes in rainfall regime simulated by GCMs increased the volume of RWR available along a year. Consequently, the transition

rates, which were defined as a function of RWR and IRW (equations 14), were increased allowing a larger expansion of agricultural areas.

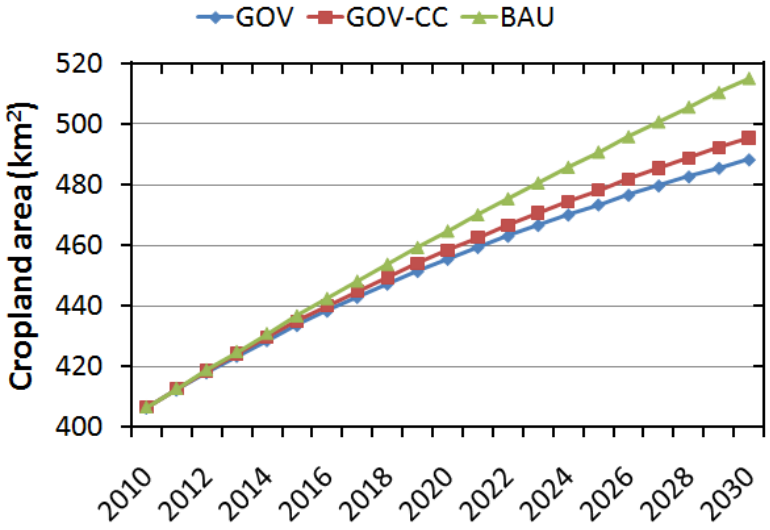

Figure 8. LUCC simulation results from 2010 to 2030.

In Figure 9, the historical land use maps for 1987 and 2003 are displayed (upper left and upper right) together with the land use maps for 2030 resulted from the BAU and GOV scenarios simulations (lower left and lower right). It is observed that in 1987 croplands were already clearly established along highlands (central area in the maps). This is explained by the favorable climatic and edaphic conditions for agricultural activities (e.g. high precipitation rates), which resulted in the clearance of large areas of forest during the last century. The remaining forests have been used for firewood collection, charcoal manufacturing and grazing (Pellikka et al., 2009).

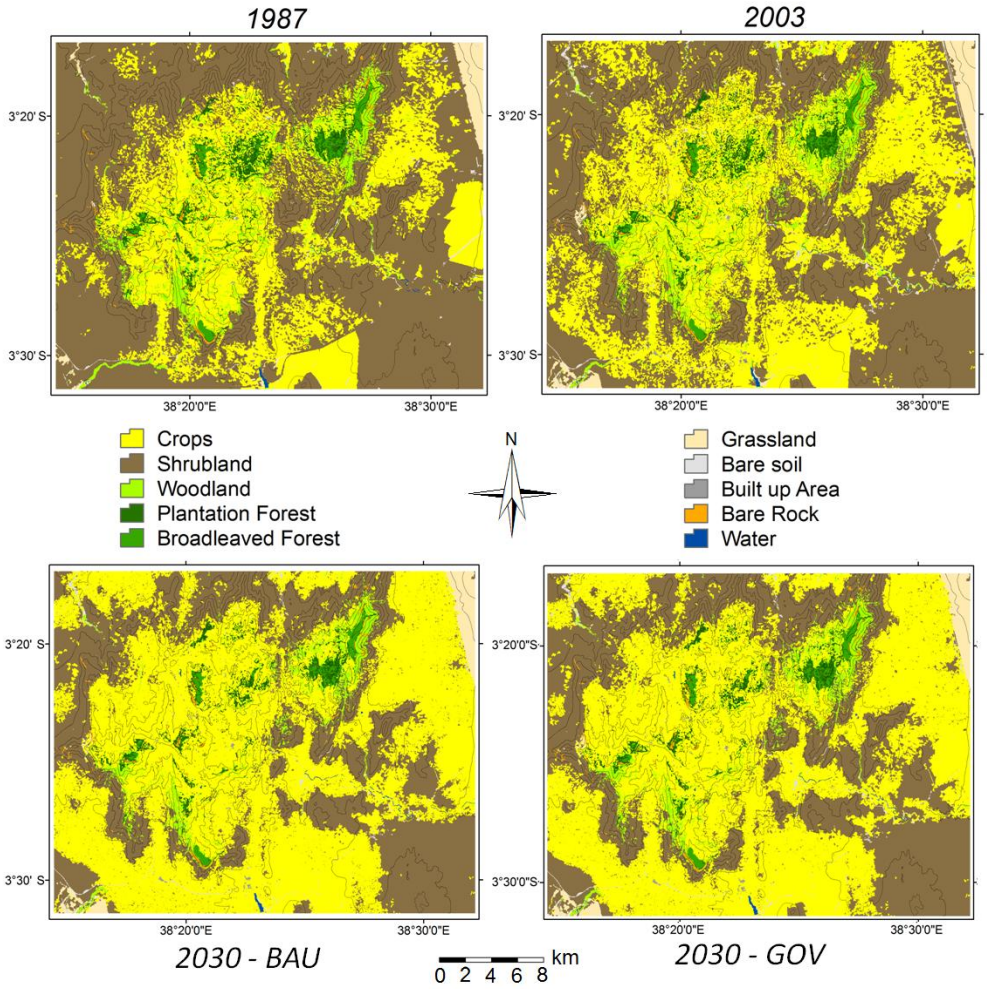

Figure 9. Historical land use maps for 1987 and 2003 (upper left and upper right) and simulated scenarios for 2030 (lower left and lower right).

Between 1987 and 2003, croplands started to be implemented with higher intensity along lowlands, provided that suitable areas for agriculture activities in highlands were already almost entirely taken. This trend is clearly reflected in the LUCC simulation results. Although each simulated scenarios was created independently, using different transitions rates, the spatial distribution of new cropland patches followed the same patterns in all simulations. As suitable agricultural areas in highland were already taken, the expansion of new patches was distributed in the length of foothills. Among the main driving forces of such distribution were the distance to markets (here represented by villages or towns), distance to roads and distance to rivers.

Distance to markets and roads played an interesting role in croplands distribution, in the sense that the effects of these two variables in the landscape dynamic were closely related. Namely, towns and villages acted as core points interconnected by roads creating axis in which new cropland patches were settled. Such patterns were observed mainly in the southern and southwestern part of the study area.

It is also important to notice the enhanced importance attributed to rivers in the land use dynamic. Given that in this region foothills typically have higher average

temperatures and lower precipitation volumes, the proximity to water bodies are essential to the establishment of agricultural activities.

4.2 ETo models assessment and calibration

A comparison between the air temperature records measured at Voi weather station and the Land Surface Temperature (LST) records obtained by the MODIS sensor is presented in Figure 10. The graphic shows the monthly averages from 2001 to 2008. The LST data were acquired from one point with the same latitude and longitude as the ground weather station. The day LST corresponds to measurements acquired around 10:30 am, while night LST records are acquired around 22:30 pm (local solar time).

A close fitness between the minimum air temperature and the night LST is observed. However, seasonal variations are noticed in the comparison between the maximum air temperatures and day LST. Such variations were already reported in literature. For instance, Mostovoy et al. (2005) observed good correlations between LST and max/min air temperatures during winter season over Mississippi. Nevertheless, a poor correlation was observed in this same area during summer season. The authors consider that this problem may be caused by the fact that green vegetation during summer period reduces a deterministic component of the relationship between LST and min/max air temperatures.

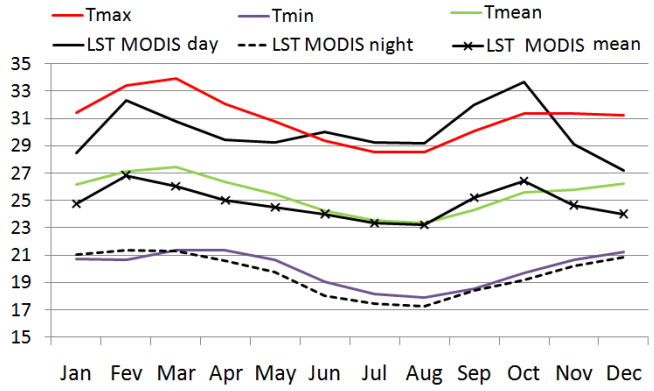

Figure 10. Monthly averages of maximum, minimum and mean air temperature measured at Voi weather station and monthly averages of day, night and mean Land Surface Temperatures (LST) retrieved from MODIS sensor (2001-2008).

The results obtained in the evaluation of the ETo models are summarized in Table 3. The RMSE and MAE were considerably different for each of the evaluated models. The average RMSE ranged from 0.57 mm.day^{-1}, with the Blaney-Cridle model, to 1.87 mm.day^{-1}, with the Thornthwaite model. The monthly RMSE and MAE for the Thornthwaite model (Figure 11) were generally high when compared with published works. For instance, in a study case carried out in the south of Iran, Ahmadi and Fooladmand (2008) achieved RMSE lower than 1 mm.day^{-1} using the Thornthwaite equation, while in the present study the results ranged from 1.4 to 2.5mm.day^{-1}. Hence, based on the results achieved in this study and in the comparison with previous researches, it was concluded that the Thornthwaite model is not the most appropriate for this study area.

Table 3. Summary of the results obtained from the models' error analysis and linear regression analysis.

	Hargreaves	***Thornthwaite***	***Blaney-Criddle***
Correlation coefficient (R)	0.67	0.66	0.55
RMSE (mm day^{-1})	1.07	1.87	0.57
MAE (mm day^{-1})	0.98	1.80	0.50
Calibration parameter (a)	3.221	3.507	-1.980
Calibration parameter (b)	0.497	0.543	1.379

The errors obtained by the Hargreaves and Blaney-Criddle models were consistent with results observed in previous published researches. The average RMSE obtained by the Hargreaves model was 1.07mm.day^{-1}, while the monthly errors ranged from 0.5 to 1.5 mm.day^{-1}. These results are compatible with the errors observed by Gavilán et al. (2006), which evaluated the Hargreaves equation under semiarid conditions in Southern Spain, finding RMSE ranging from 0.46 to 1.65mm.d^{-1}.

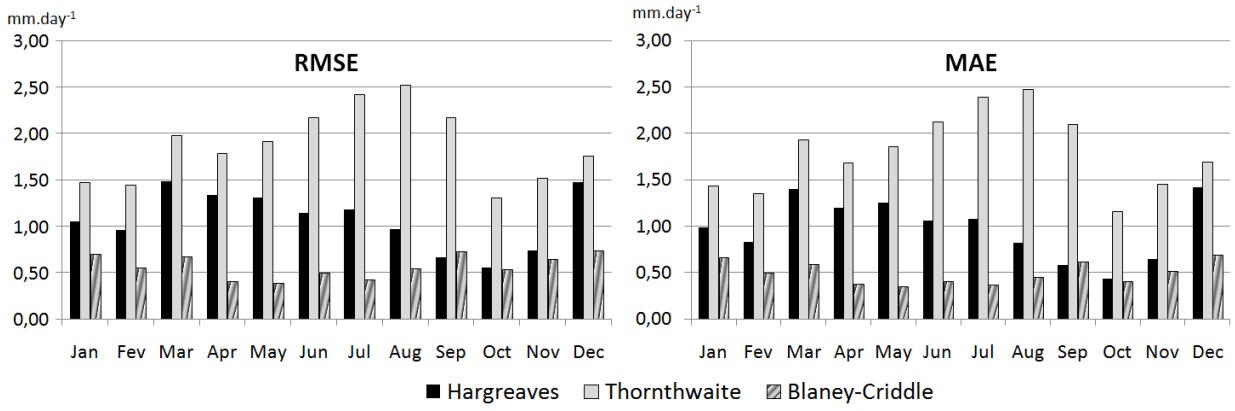

Figure 11. Root Mean Squared Error (RMSE) and Mean Absolute Error (MAE) achieved by ETo models evaluated

The Blaney-Criddle model, in turn, achieved an average RMSE of 0.57 mm.d^{-1} and a MAE of 0.50 mm.d-1, representing the best results obtained by the models when taking into account these criteria. However, as can be observed from Table x, the correlation coefficient of 0.55 obtained from a linear regression with the FAO-PM method was much lower than the ones achieved by the other models. Such correlation is low when compared with previously published results. For instance, Fooladmand and Ahmadi (2009) found correlation coefficients up to 0.96 in the linear regression analysis between the Blaney-Criddle and the FAO-PM methods applied in the south of Iran.

It is worth mentioning that the results obtained by Fooladmand and Ahmadi (2009), Ahmadi and Fooladmand (2008) and Gavilán et al. (2006) were achieved

using the same input in every evaluated model (i.e. Hargreaves, Thornthwaite and Blaney-Criddle) and in the reference model (i.e FAO-PM). That is to say, all models in these quoted works were parameterized using weather data from ground stations, while in the particular case of this work the analyzed models were parameterized using LST data obtained from the MODIS sensor and the FAO-PM model using weather data from a ground station.

The fitted regression lines and the normal probability plot of the residuals resulting from the linear regression analysis are displayed in Figures 12 and 13, respectively. The correlation coefficients obtained by the Hargreaves and Thornthwait models are consistent with the results reported by Narongrit and Yasuoka (2003), which achieved R^2 of 0.57 and 0.60 when comparing these respective models with the FAO-PM method.

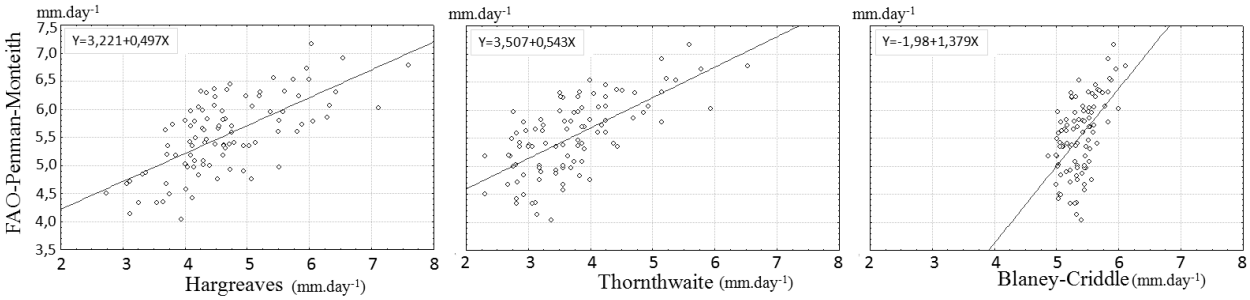

Figure 12. Fitted regression lines comparing the results obtained by evaluated models with the reference values calculated by the FAO-PM model.

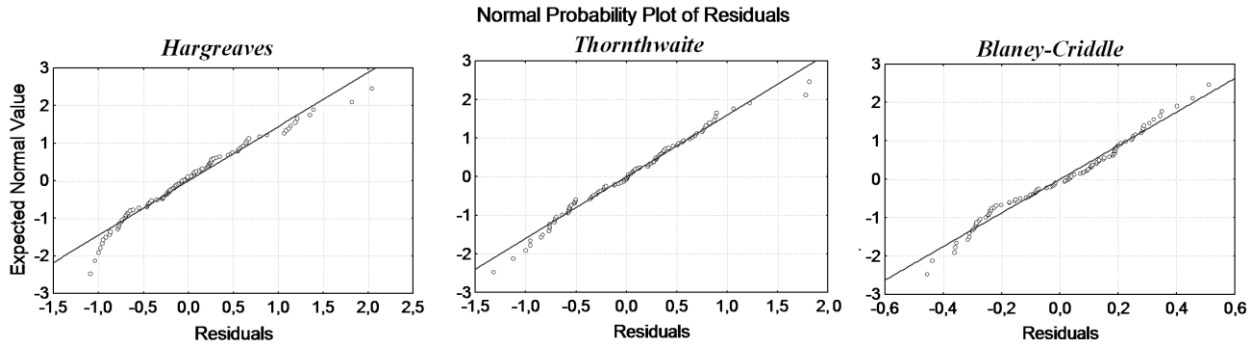

Figure 13. Normal probability plots resulted from the linear regression analysis.

Finally, considering the error analysis and the linear regression analysis, the Hargreaves model was chosen for this study. Thus, having in hand the chosen model with its respective calibration parameters and the input data acquired by the MODIS sensor, it was possible to represent the spatial-temporal distribution of the ETo in the study area. Figure 14 illustrates the monthly average ETo maps created using as baseline LST records from 2001 to 2008, which were used in simulating the scenarios described in the presented work.

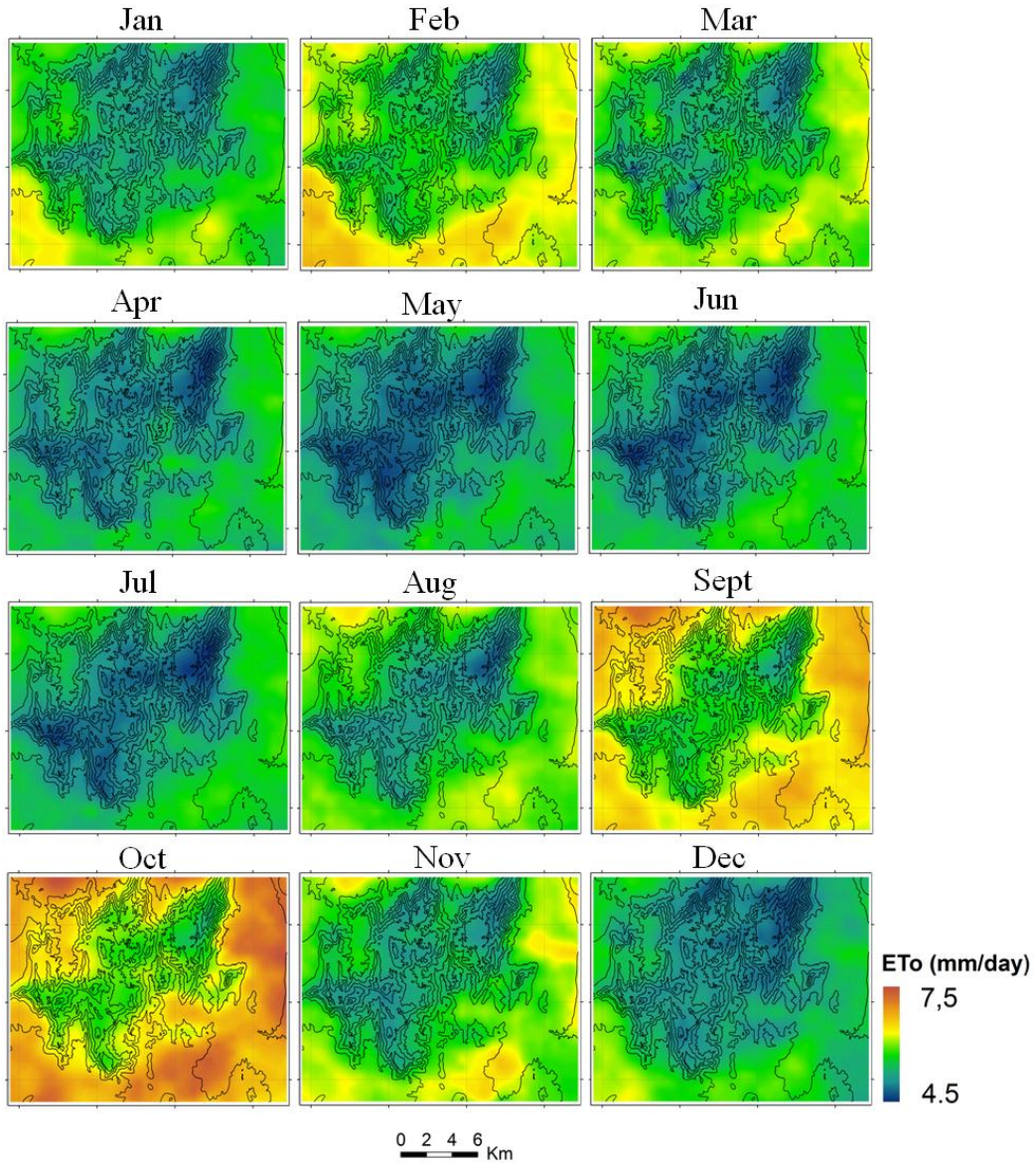

Figure 14. Monthly average Reference Evapotranspiration (ETo) maps obtained using the Hargreaves model and LST records from 2001 to 2008.

4.3 Spatial-Temporal distribution of Crop coefficients (kc)

The first step carried out in defining the Crop Coefficients (kc) was the identification of the agricultural calendar in the study area, that is to say, the identification of the crops seeding season, growing season and harvest. For this, 150 random points were distributed along the areas classified as croplands in the year 2003 (Figure 15). The year 2003 was chosen for having the most recent high resolution land use and land cover mapping for this study site.

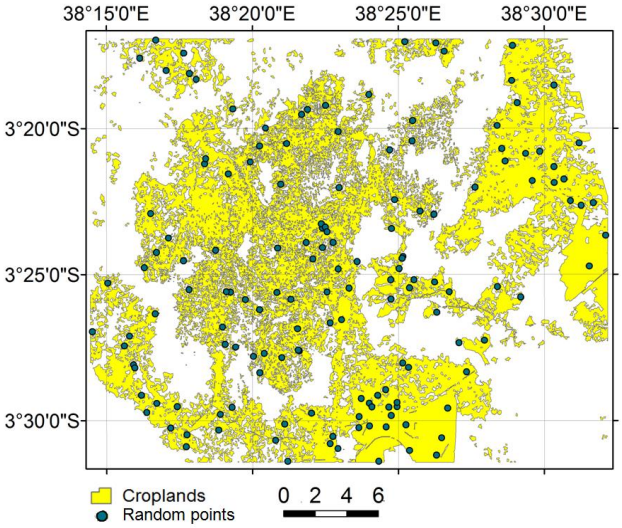

Figure 15. random points distributed along the cropland areas.

Next, the random points were overlapped with monthly NDVI images obtained by the MODIS/Terra-Aqua sensors. The monthly NDVI images were compiled using the entire MOD13Q1 product dataset from 2001 to 2008 (Figure 16). Because the MODIS/NDVI images have a spatial resolution of 250 meters and the agricultural activities in this area consist predominantly of small properties, the frequency of pixel mixture is likely very high. Hence, a pixel purity analysis was performed in the MODIS imagery and from the 150 points randomly distributed only 50 points with the highest pixel purity index were chosen to characterize the NDVI profile of croplands.

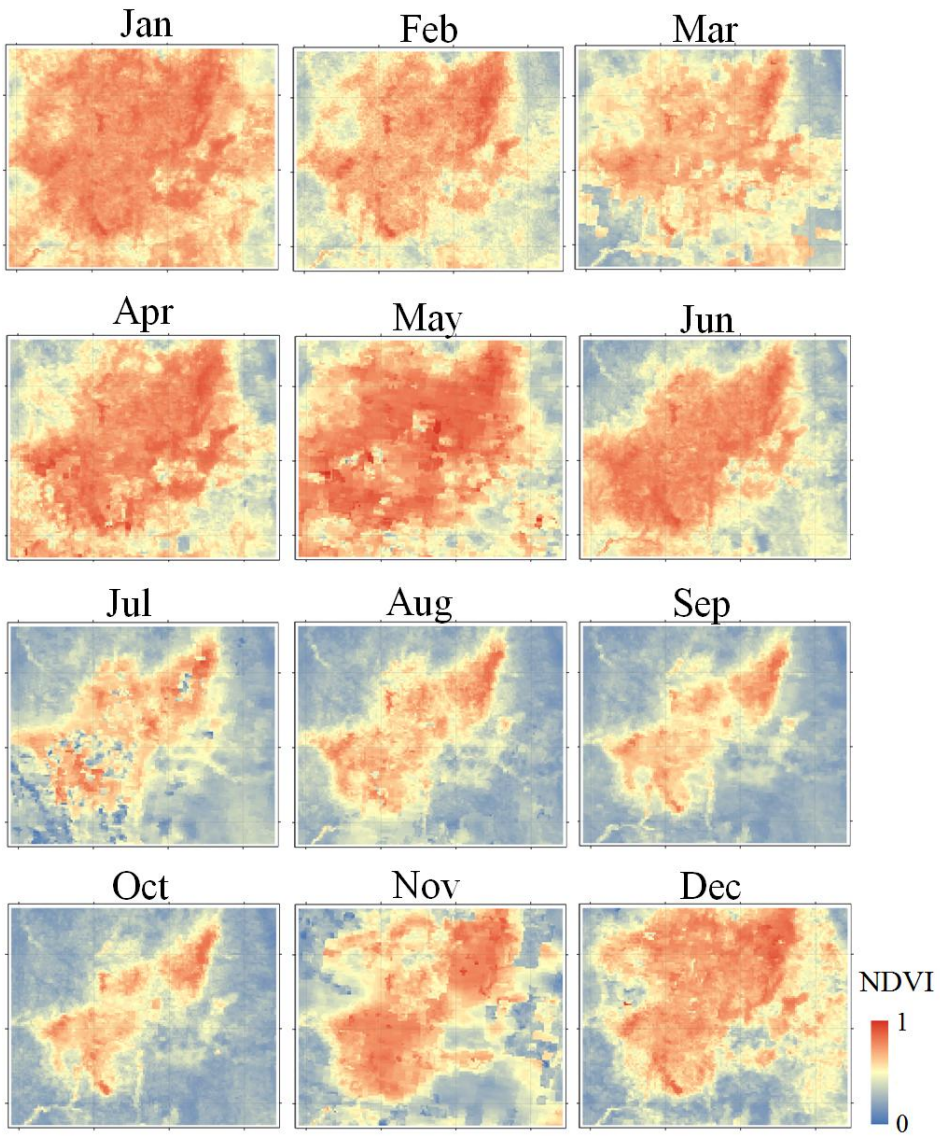

Figure 16. MODIS monthly NDVI images, representing the averages from the years 2001 to 2008.

The NDVI temporal profile from croplands is displayed in Figure 17a. Two crop seasons can be identified based on the vegetation phenology captured by the NDVI. A clear seeding season is observed from August to October, when NDVI values reach the lowest values. The first growing season happens between October and January, when a clear increase in the NDVI values take place. These values decrease again from January to February, indicating crops' senescence period. The NDVI values are kept low between February and March, when the crops harvest is taking place together with a new seeding season. And finally, from March to August a new agricultural cycle takes place.

The observations exposed above are confirmed by agricultural calendars provided by Kenya's Ministry of Agriculture (Jaetzold, and Schmidt, 1983), which are presented in Figures 17b and 17c. Figure xb shows the Maze seeding activities in Taita tarveta district, where two clear seeding seasons are evident with it peak happening on March and October. The harvest seasons happen mostly in February and between June and July (Figure 17c).

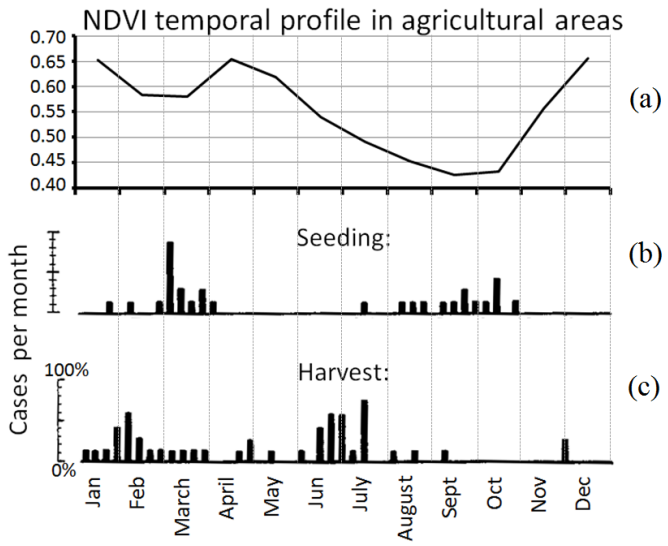

Figure 17. (a) NDVI temporal profile from cropland areas; (b) Maze seeding calendar in Taita Tarveta district; (c) Maze harvest calendar in Taita Tarveta district (source: Jaetzold, and Schmidt, 1983).

After the agricultural calendar was identified, Kc values were attributed for each crop growth stage based on values recommended by the FAO (Allen et al., 1998). This procedure is illustrated in Figure 18, which shows a comparison between the NDVI temporal profile from cropland areas and the monthly Kc values used in this study.

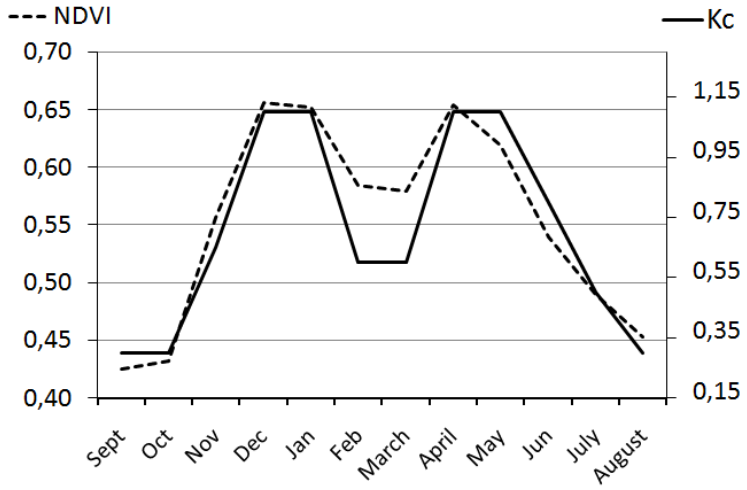

Figure 18. Comparison between the NDVI temporal profile from cropland areas and the monthly Kc values used in this study.

4.4 Irrigation water requirement (IWR) assessment

The annual IWR volumes resulting from the scenarios simulation are presented in Figure 19. The final simulation results for the year 2030 are summarized in Table 4,

together with estimated IWR values for 1987 and 2003. The BAU scenario showed the highest IWR, reaching aproximetely 236 million $m^3.year^{-1}$ in the year 2030. In the governance scenario inserted in the same climate conditions, the IWR was reduced in approximately 1%, representing a decrease of 12 million $m^3.year^{-1}$. On the other hand, the GOV-CC scenario retrieved the lowest IWR by 2030. Hence, the results indicate that the climate changes simulated by the GCMs are likely to decrease the total annual volume of IWR in this study area. These results differ from those obtained by studies performed in different regions of the globe. For instance, studying the Guadalquivir river basin in Spain, Diaz et al. (2007) found that climate changes may result in increases between 15 and 20% in seasonal irrigation need by the 2050s.

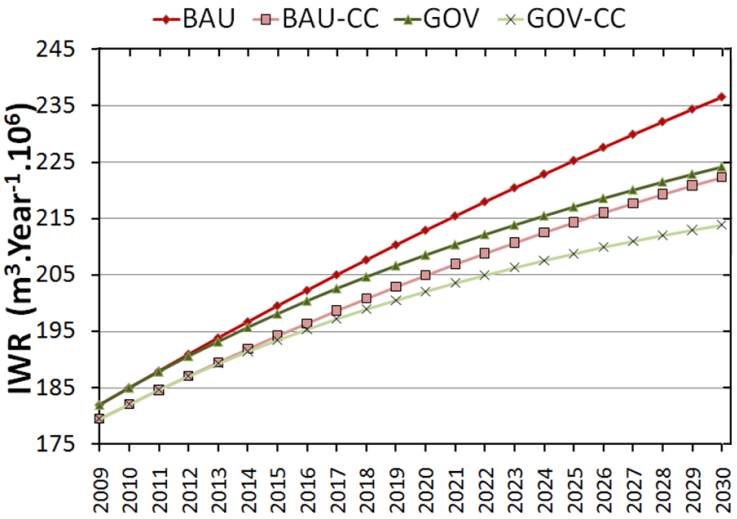

Figure 19. Simulated scenarios of Irrigation water requirements for Taita hills.

Table 4. Summary of the results obtained in the IWR simulations

	10^6 cubic meters
Annual precipitation volume (entire study area)	389.98
Annual IWR volume - 1987	110.32
Annual IWR volume - 2003	163.12
Annual IWR volume – 2030 - BAU	236.54
Annual IWR volume – 2030 – BAU-CC	222.32
Annual IWR volume – 2030 – GOV	224.19
Annual IWR volume – 2030 – GOV-CC	213.87

In Figure 20 a comparison example between the land use maps and IWR maps is presented. As previously discussed, the highlands located in the central region of the study site were already almost totally used for agricultural activities by 1987 and 2003. This particular aspect of the landscape dynamic in this region is

easily comprehensible when analyzing the ETo maps from Figure 14, and the IWR maps from Figure 20. The milder temperatures and higher precipitation rates in the hills areas result in lower potential ET rates, making agricultural activities more attractive, given that less water is required for irrigation. As such regions were saturated, croplands started to expand to the vicinities of urban areas and roads in the foothills, also attempting for the proximity to water bodies.

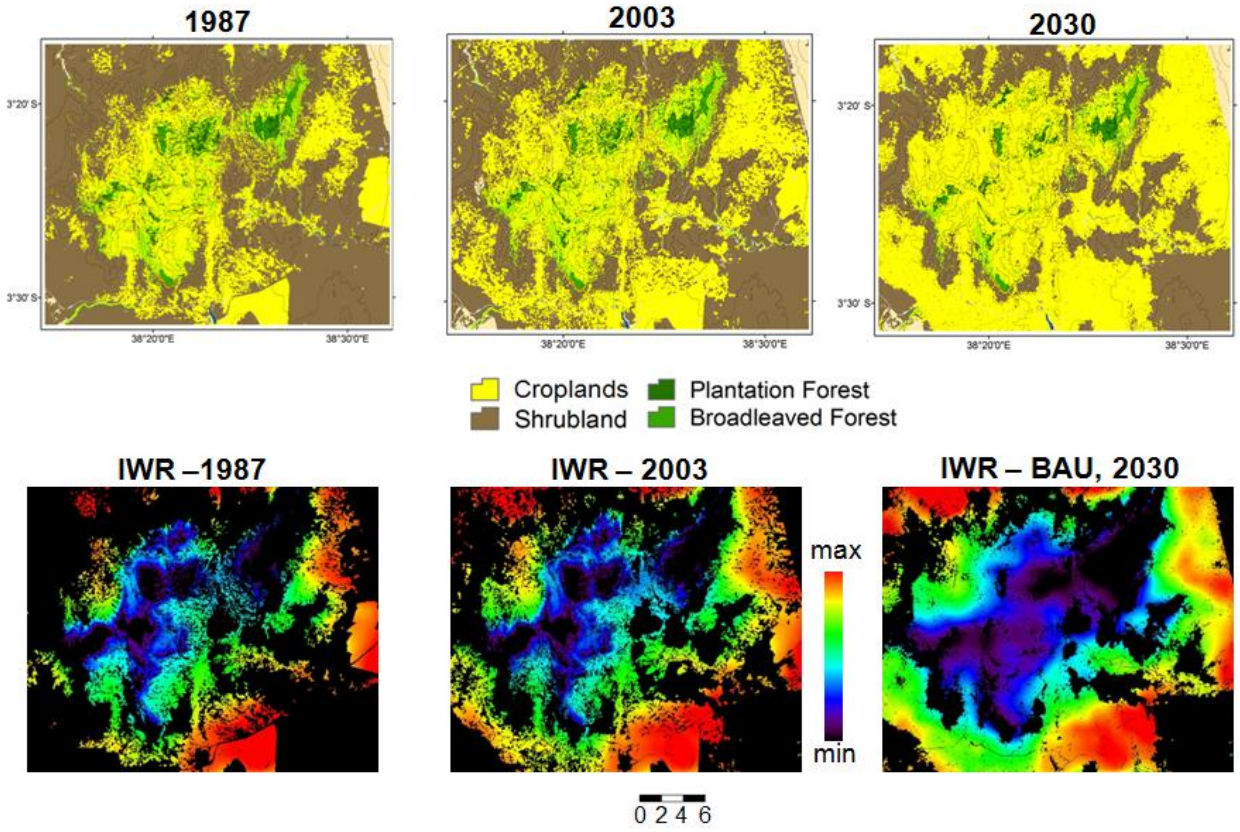

Figure 20. Comparisson between the land use maps and IWR simulations.

As a consequence, from 1987 onwards areas with higher average ETo started to be used for agriculture. Such fact is clearly illustrated in the histogram presented in Figure 21. From 1987 to 2003 a large number of cropland patches were created in areas with ETo between 5.7 and 5.9 mm.day^{-1}, while very few new patches were implemented in areas with lower ETo. This tendency was sustained during all scenarios simulations until 2030. Hence, it is feasible to state that in the next 20 years new agricultural properties will likely require higher water volumes for crop production in order to achieve the same yield as croplands previously installed in highlands.

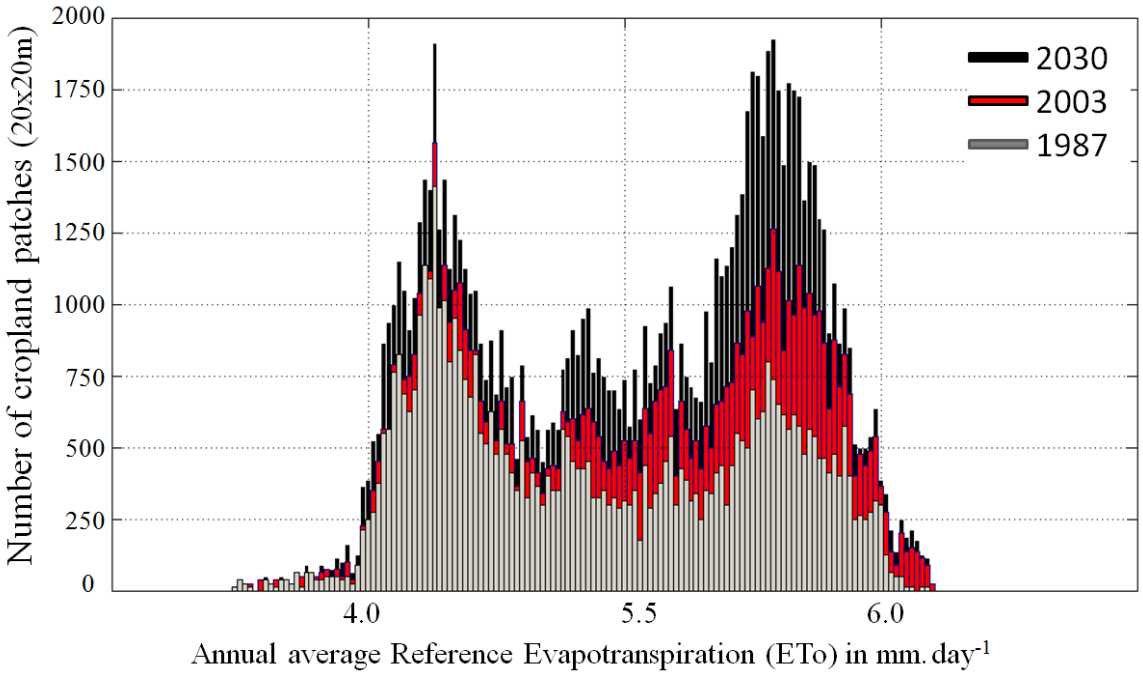

Figure 21. Histogram showing the cropland patches distribution during 1987, 2003 and 2030, in relation to the average ETo in the study area.

The average monthly IWR distributions simulated for 2030 are displayed in Figure 22. Carrying out an intrannual analysis it is possible to observe that between May and October the scenarios accounting for climate change (BAU-CC and GOV-CC) have a negative impact on IWR, that is, during this period the climate changes simulated by the GCMs are expected to slightly increase IWR. Nevertheless, this effect is compensated in the remaining months of the year in a much higher magnitude, resulting in an overall positive effect, in which the annual average IWR for the scenarios with climate change are significantly lower than the scenarios not accounting for changes in climate.

In all scenarios, the highest IWR peak happens in January, which coincides with the maximum development of crops during the first growing season. Along January and December the highest differences between scenarios are observed, reflecting a higher uncertanty during these periods of the year.

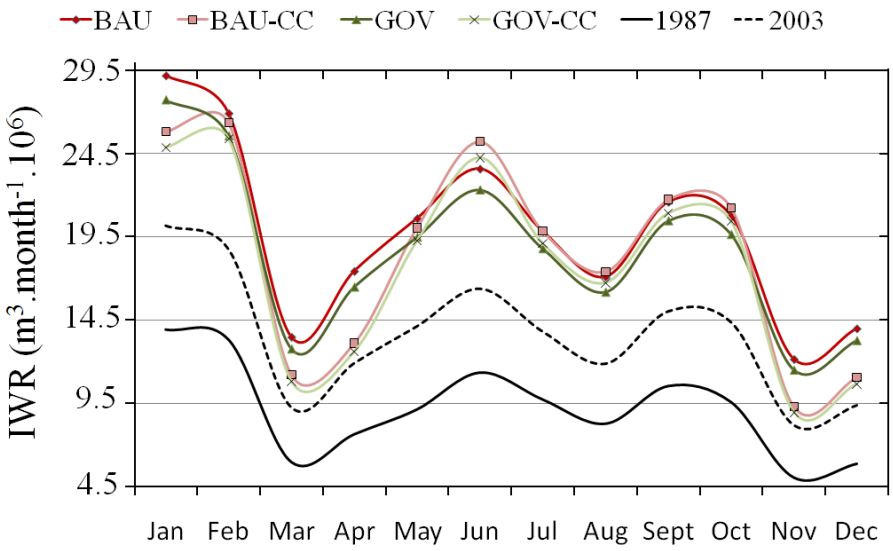

Figure 22. Monthly IWR distribution for 1987, 2003 and all the 2030 scenarios

In Figure 23, the monthly IWR maps illustrates the spatial-temporal aspect of the IWR distribution throughout the year 2030 for the BAU scenario. During December, January and February the highest IWR values are clearly distributed along the south and southwest foothills, while during May, June and July the east and southeast regions show the highest values.

Along almost the entire year, a clear distinction can be made between the IWR values in highlands and lowlands. However, this distinction is curiously reduced during July, August and September, when the IWR distribution in the study area becomes more homogeneous.

Consequently, two important aspects can be highlighted from the results of this study. Firstly, the construction of LUCC and IWR scenarios at a high spatial resolution offers an unquestionable tool for local decision makers in identifying priority areas from the point of view of land use allocation and water resources policy. Secondly, the development of a methodology based on a ET model with local calibration can benefit local stakeholders in the direction of a proper irrigation water management, avoiding conflicts, water scarcity and environmental consequences.

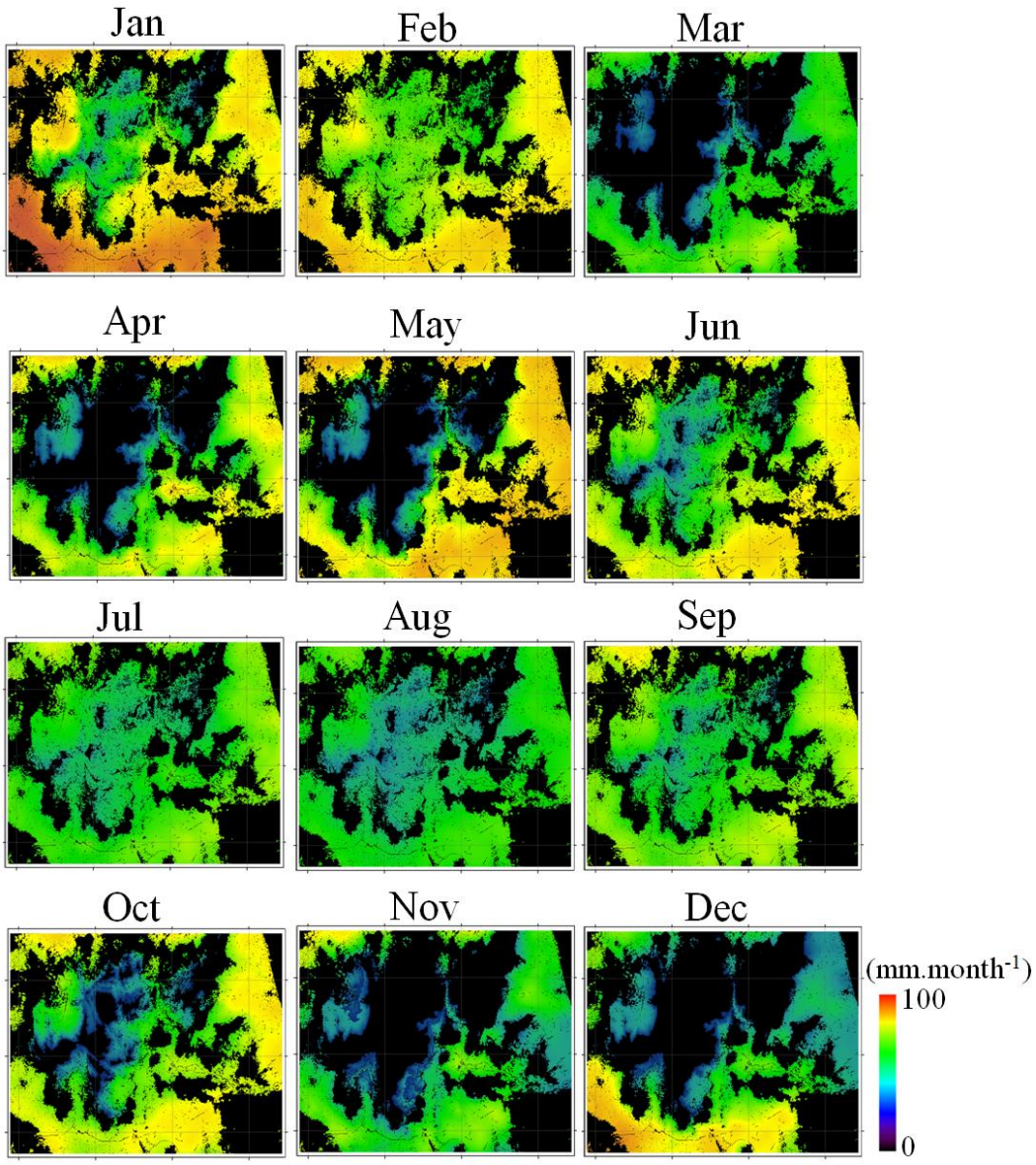

Figure 23. Monthly IWR maps for 2030 - BAU scenario

5. Conclusions

The presented research was successful in identifying the main landscape variables affecting the landscape dynamic in the study area. A connected relation between villages and roads is evident in the definition of new cropland patches. LUCC simulations indicate that agricultural expansion will likely take place predominantly in lowlands and foothills throughout the next 20 years. Such dynamic will increase the spatial dependence on distance to rivers and other water bodies due to the higher potential ET in these areas. If current trends persist, it is expected that agricultural areas will occupy 60% of the study area by 2030.

The results of the LUCC simulations described in this research have good potential to be used by policy makers in improving the identification of priority regions from the point of view of land use allocation and environmental risks. Moreover, it renders an important tool for researchers to understand the human-environment relations in this region.

Based on the analysis of RMSE, MAE and linear regression analysis, the Hargreaves ETo model was selected as the most appropriate for this particular study area. The LST data acquired by the MODIS sensor was successfully used as input for the chosen ETo model, retrieving an average RMSE close to 1 $mm.d^{-1}$, which is consistent with results obtained by previous studies reported in the literature. Moreover, the errors and uncertainties identified in the use of remote sensing LST can be tolerated considering the reduced weather data collection network in Taita hills. Further studies should be considered in order to expand this method for the entire East-Africa. In particular, the Hargreaves model should to be tested for its suitability in the different climate conditions and the spatial variability of the calibration parameters needs to be identified.

In East-Africa, the low availability of weather data from ground stations is a limiting factor for using standard ET calculation approaches. This fact, associated with poverty and inadequate water management techniques, aggravates the water scarcity condition faced in this region. On the other hand, the MODIS-Terra/Aqua sensor offers almost daily LST data, which can be easily downloaded from internet. Therefore, the methodology presented in this study can be considered a feasible and cost free alternative for estimating ETo. The operational use of such method has good potential for improving water distribution by allowing an increased control on water use for irrigation.

The results obtained by the modeling framework assembled in the presented study indicate that by 2030 climate changes simulated by GCMs will likely decrease IWR when compared with a scenario that uses the same temperature and precipitation averages as in the historical dataset. The approach used in this study can effectively represent the spatial-temporal aspects of the IWR distribution along the study area. Due to the low availability of space in highlands, new cropland areas are being settled in areas with low precipitation and higher temperatures. The continuity of this trend, as simulated by the models, will result in new agricultural areas with higher IWR and consequently, an increasing pressure on water resources.

The management of water use for irrigation is a task that requires long-term planning. At the same time, the consequences involved in the inappropriate use of water resources also have long-term implications. In this context, the future IWR scenarios simulated within this study is an important asset to identify emerging trends and support informed strategic decisions.

Finally, further works are required to improve the results obtained in this study. Namely, the consistency of the Monte Carlo simulations to construct synthetic weather datasets can be improved by defining site-specific probability distribution functions for temperature and precipitation. Additionally, local ET measurements, using direct methods, would improve the model's calibration. Nevertheless, the data acquisition necessary to carry out such tasks is evidently time consuming and requires significant amount of financial resources.

6. References

Alcamo, J., 2001, Scenarios as tools for international environmental assessments, Experts corner reports - Prospects and Scenarios No 5. European Environment Agency, Copenhagen.

Allen, R.G, Pereira, L.S., Raes, D. and Smith,M., 1998: Crop evapotranspiration - Guidelines for computing crop water requirements - FAO Irrigation and drainage paper 56, FAO, Rome

Ahmadi, S. H., and Fooladmand, H. R., 2008. Spatially distributed monthly reference evapotranspiration derived from the calibration of Thornthwaite equation: a case study, South of Iran. Irrigation Science, 26 (4), 303-312.

Barrios, S., Ouattara, B., Strobl, E. 2008. The impact of climatic change on agricultural production: Is it different for Africa? Food Policy, 33, 287 - 298.

Blaney, H. F., Criddle, W. D. 1962. Determining Consumptive Use and Irrigation Water Requirements. USDA Technical Bulletin 1275, US Department of Agriculture, Beltsville.

Bonham-Carter, G., 1994, Geographic information systems for geoscientists: Modelling with GIS. Elsevier Science, Pergamon, Kidlington.

Boardman, J. W., and Kruse, F. A., 1994, Automated spectral analysis: a geological example using AVIRIS data, north Grapevine Mountains, Nevada: in Proceedings, ERIM Tenth Thematic Conference on Geologic Remote Sensing, Environmental Research Institute of Michigan, Ann Arbor, MI, pp. I-407 - I-418.

Brouwer, C., Heibloem, M., Irrigation Water Management. Training Manual (FAO), no. 3 / Rome (Italy), FAO , 1986 , Prov. ed., 60 p.

Cai J., Liu Y., Lei T., Pereira L.S. 2007Estimating reference evapotranspiration with the FAO Penman-Monteith equation using daily weather forecast messages. Agricultural and Forest Meteorology, 145 (1-2), pp. 22-35.

Doorenbos J, Pruitt WO. 1977. Guidelines for Predicting Crop Water Requirements. FAO Irrigation and Drainage Paper, No. 56, FAO, Rome.

Douglas, E. M., Jacobs, J. M., Sumner, D. M., Ray, R. L., 2009. A comparison of models for estimating potential evapotranspiration for Florida land cover types. Journal of Hydrology, 373 (3-4), 366-376.

Díaz R. J., Weatherhead, E., Knox, J., Camacho, E. 2007. Climate change impacts on irrigation water requirements in the Guadalquivir river basin in Spain. Regional Environmental Change, 7 (3), 149-159.

FAO - Food and Agriculture Organization of the United Nations, Land and Water Development Division. Irrigation potential in Africa: A basin approach, FAO , 1997, 177p.

FAO - Food and Agriculture Organization of the United Nations, Land and Water Development Division. 2005. AQUASTAT Information System on Water and Agriculture: Online database. Rome: FAO.

Fooladmand, H. R., Ahmadi, S. H., 2009. Monthly spatial calibration of Blaney-Criddle equation for calculating monthly ETo in south of Iran. Irrigation and Drainage, 58 (2), 234 – 245.

Gavilán, P., Lorite, I.J., Tornero, S., Berengena, J., 2006. Regional calibration of Hargreaves equation for estimating reference ET in a semiarid environment. Agriculture Water Management 81, 257–281.

Hagen, A., 2003, Fuzzy set approach to assessing similarity of categorical maps. International Journal of Geographical Information Science, 17(3), pp. 235–249.

Hargreaves, G.H., Samani, Z.A., 1985. Reference crop evapotranspiration from temperature. Appl. Eng. Agric. 1 (2), 96–99.

Itenfisu, D., Elliott, R.L., Allen, R.G.,Walter, I.A., 2003. Comparison of reference evapotranspiration calculation as part of the ASCE standardization effort. Journal of Irrig. Drain. Eng. ASCE 129 (6), 440–448.

Jabloun, M., Sahli, A., 2008. Evaluation of FAO-56 methodology for estimating reference evapotranspiration using limited climatic data. Application to Tunisia. Agricultural Water Management, 95 (6), 707-715.

Jaetzold, R., Schmidt, H., 1983. Farm Management Handbook of Kenya, vol. II. East Kenya. Ministry of Agriculture, Kenya.

Justice, C.O., Townshend, J.R.G., Vermote, E.F. et al., 2002, An overview of MODIS Land data processing and product status. Remote Sensing of Environment, 83, pp. 3-15.

Loukas A, Vasiliades L, Domenikiotis C, Dalezios NR. 2005. Basin-wide actual evapotranspiration estimation using NOAA/AVHRR satellite data. Physics and Chemistry of the Earth 30: 69–79.

Mohan S, Arumugam N. 1995. An intelligent front-end for selecting evapotranspiration estimation methods. Computers and Electronics in Agriculture 12: 295–309.

Mostovoy, G.V., R. King, K.R. Reddy and V.G. Kakani. 2005. Using MODIS LST data for high-resolution estimates of daily air temperature over Mississippi. Proceedings of the 3rd international workshop on the analysis of multi-temporal remote sensing images, IEEE, CD Rom, 76 – 80.

Narongrit, C. and Yasuoka, Y., 2003. The Use of Terra-MODIS Data for Estimating Evapotranspiration and Its Change Caused By Global Warming. Environmental Informatics Archives, 1, 505-511.

Oki, T. and Kanae, S., 2006. Global Hydrological Cycles and World Water Resources. Science 313 (1068), 1068-1072.

Pellikka, P, M. Lötjönen, M. Siljander & L. Lens. 2009. Airborne remote sensing of spatiotemporal change (1955–2004) in indigenous and exotic forest cover in the Taita Hills, Kenya. International Journal of Applied Earth Observation and Geoinformation, 11(4), 221-298.

Republic of Kenya, 2001. The 1999 Population & Housing Census. Central Bureau of Statistics, Ministry of Planning and National Development, Kenya.

Rockstrom, J., Falkenmark, M., Karlberg, L., Hoff, H., Rost, S., Gerten, D., 2009. Future water availability for global food production: The potential of green water for increasing resilience to global change. Water Resources Research, 45, W00A12, doi:10.1029/2007WR006767

Rodrigues, H. O., Soares-Filho, B. S., Costa, W. L. S., 2007. Dinamica EGO, uma plataforma para modelagem de sistemas ambientais. In: Simpósio Brasileiro de Sensoriamento Remoto, 13, 3089-3096.

Soares-Filho, B.S., Pennachin, C.L., Cerqueira, G., 2002, DINAMICA – a stochastic cellular automata model designed to simulate the landscape dynamics in an Amazonian colonization frontier. Ecological Modelling, 154(3), pp. 217-235.

Soares-Filho, B. S., Garcia, R. A., Rodrigues, H. O., Moro, S., Nepstad, D., 2007. Coupling socioeconomic and demographic dimensions to a spatial simulation model of deforestation for the Brazilian Amazon. In: LBA-ECO 11th Science Team Meeting.

Thornthwaite, C. W., 1948. An approach toward a rational classification of climate. Geographical Review, 38, 55–94.

Townshend, J. R. G., and Justice, C. O., 1988, Selecting the spatial resolution of satellite sensors required for global monitoring of land transformations, International Journal of Remotes Sensing, 9, 187-236.

Wagner, S., Kunstmann, H., Bárdossy, A., Conrad, C., and Colditz, R. R. 2008. Water balance estimation of a poorly gauged catchment in West Africa using dynamically downscaled meteorological fields and remote sensing information. Physics and Chemistry of the Earth, 34 (4-5), 225-235.

Wan, Z. 2008. New refinements and validation of the MODIS land-surface temperature/emissivity products, Remote Sensing of Environment, 112, 59-74.

Veldkamp, T. and Lambin, E. F., 2001. Predicting land-use change. Editorial. Special issue. Agriculture, Ecosystems & Environment , 85 (1-3), 1-6.